DOI: 10.1002/chem.200701036

Dispirofluorene–Indenofluorene Derivatives as New Building Blocks for Blue Organic Electroluminescent Devices and Electroactive Polymers

Cyril Poriel,*[a] Jing-Jing Liang,[a] Joëlle Rault-Berthelot,*[a] Frédéric Barrière,[a] Nicolas Cocherel,[a] Alexandra M. Z. Slawin,[c] David Horhant,[a] Morgane Virboul,[a] Gilles Alcaraz,[a, d] Nathalie Audebrand,[a] Laurence Vignau,*[b] Nolwenn Huby,[b] Guillaume Wantz,[b] and Lionel Hirsch[b]

Abstract: A series of new dispiro[fluorene-9′,6,9″,12-indeno[1,2b]fluorenes] (DSF-IFs) has been synthesised. These new building blocks for blue-light-emitting devices and electroactive polymers combine indenofluorene (IF) and spirobifluorene (SBF) properties. We report here our synthetic investigations towards these new structures and their thermal, structural, photophysical and electrochemical properties. These properties have been compared to those of IF and SBF. We also report the anodic oxidation of DSF-IFs that leads to the formation of non-soluble transparent three-dimensional polymers. The structural and electrochemical behaviour of these polymers has been studied. The first application of these building blocks as new blue-light-emitting materials in organic light-emitting diodes (OLED) is also reported.

Keywords: cyclic voltammetry · dispirofluorene–indenofluorene · fluorescence · light-emitting diodes · polymers

Introduction

During the last two decades, organic light-emitting diodes (OLEDs) have attracted considerable interest owing to their promising applications in flat-panel displays that could replace cathode-ray tubes or liquid-crystal displays.[1] The ability to mass produce thin, efficient, bright displays from organic polymers and small molecules that can supplant modern liquid-crystal technology depends almost entirely on the ability to create new materials that can undergo efficient electroluminescence in a wide range of wavelengths. In terms of revenue, 2005 and 2006 have been the breakthrough years for the OLED technology in small- and medium-size displays. However, its market penetration is expected to remain modest in 2007.[2] This mainly arises from the rather short lifetime of organic materials despite the recent years improvements. Indeed, a number of approaches have been tried for producing full-colour displays, for example, in fabricating red, green and blue pixels. However, the shorter lifetime of the blue-emitting materials is still one the main problem in OLED technology.[2] In this context, the quest for a material, for example, polymers[3–17] or small molecules,[18–46] with stable blue emission within an electroluminescent device continues to hold the attention of number of research groups. It is of course not an easy task to find a small molecule that not only possesses a very large band gap, a large quantum yield in the solid state and that is also stable to the harsh OLED environment. Fluorene (F) derivatives have been the most studied materials for blue emis-

[a] Dr. C. Poriel, J.-J. Liang, Dr. J. Rault-Berthelot, Dr. F. Barrière, N. Cocherel, Dr. D. Horhant, M. Virboul, Dr. G. Alcaraz, Dr. N. Audebrand
UMR CNRS 6226 "Sciences Chimiques de Rennes"
Université de Rennes 1, Bat 10C, Campus de Beaulieu
35042 Rennes cedex (France)
Fax: (+33)223-236732
E-mail: cyril.poriel@univ-rennes1.fr
joelle.rault-berthelot@univ-rennes1.fr

[b] Dr. L. Vignau, Dr. N. Huby, Dr. G. Wantz, Dr. L. Hirsch
UMR CNRS 5218 Université de Bordeaux
ENSCPB, 16 Avenue Pey-Berland, 33607 Pessac cedex (France)
Fax: (+33)540-006631
E-mail: l.vignau@enscpb.fr

[c] Prof. A. M. Z. Slawin
School of Chemistry, University of St Andrews
St Andrews, Fife KY16 9ST (UK)

[d] Dr. G. Alcaraz
Laboratoire de Chimie de Coordination (LCC)
UPR CNRS 8241, Equipe A. O. C., 205 route de Narbonne
31077 Toulouse Cedex 04 (France)

Supporting information for this article is available on the WWW under http://www.chemeurj.org/ or from the author.

sion, and this has led to many publications and patents. However, up to now, this has failed to produce an efficient, cheap and robust blue-light emitters.[2,33] Since the electronic and optical characteristics of the rigid F arise from its planar biphenyl moieties, the structurally related compound, indenofluorene (IF), with a planar, longer conjugated p-terphenyl moieties has been suggested as a promising building block. Indeed, its incorporation into polymer or oligomer backbones instead of F units has recently led to a strong enhancement of OLED properties.[3,6,25,47–50] Moreover, it is known that spiro-linked molecules such as spirobifluorene (SBF)[51] exhibit greater morphological stability and more intense fluorescence, without any significant change in their absorption and fluorescence spectra compared to the non-spiro-linked parent compounds.[28] Another highly important characteristic, which holds for most of SBF compounds, is that they do not exhibit any emission bands beyond 500 nm. Such parasite emission bands are usually found in polyfluorenes after annealing and are usually assigned to chain defects arising to partial oxidation of fluorene units.[16] We thus decided to desiGn a new family of chromophores that combine the IF and F properties within a single molecule through a spiro linkage. This new family of molecules has been called dispirofluorene–indenofluorene (DSF-IF).[52] The molecular design adopted in these molecules preserve

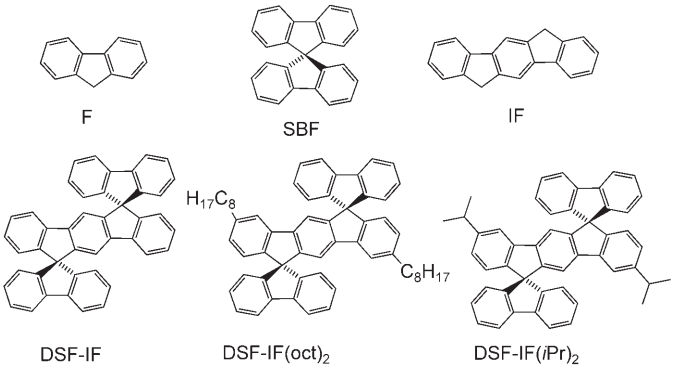

the π conjugation of the IF, which plays a prominent role in the electronic, electrochemical and photophysical properties; the introduction of the spiro configuration[51] gives the molecules a highly rigid structure.

In this work, as a development to our preliminary note,[53] we first report our synthetic investigations and a new straightforward route to the diiodoterphenyl as key building block in the synthesis of DSF-IFs. The thermal, structural, photophysical and electrochemical properties of these molecules will be discussed, together with their first application in electroluminescent devices. In addition, these versatile molecules also have the potential to form polymers by electrochemical oxidation leading to transparent electroactive deposits with interesting electrochromic properties. The structural and electrochemical behaviours of these polymers will be also developed.

Results and Discussion

Synthesis of DSF-IF derivatives

Retrosynthetic analysis: SBF can be considered as the joining of two fluorene units through a shared spiro carbon. First described by Clarkson and Gomberg in 1930,[54] it was readily obtained in a two-step synthesis from 2-iodobiphenyl and fluorenone through a metal–halogen exchange reaction.[55–58] As DSF-IF can be considered as the joining of two SBF moieties through a shared phenyl ring, it seemed reasonable to adopt a similar strategy. Our retrosynthetic approach, based on a double lithium–halogen exchange reaction, is presented in Scheme 1 and involved 2,2″-di-

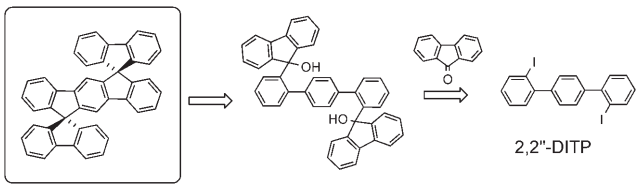

Scheme 1. Retrosynthetic analysis of DSF-IF.

iodo[1,1′;4′,1″]terphenyl (2,2″-DITP) as the key starting material. It should be noted that dihalogenated-*p*-terphenyls are not readily accessible and the target 2,2″-diiodo[1,1′;4′,1″]terphenyl has only been reported once so far.[59]

Synthesis of 2,2″-DITP: As it was crucial in our strategy to develop an efficient synthesis of 2,2″-DITP at the multigram scale, two approaches were developed, both starting from commercially available 2-iodoaniline (Scheme 2, routes 1 and 2). To avoid long and sophisticated multistep syntheses, the first method we developed involved original arylboronic acids bearing a triazene moiety in the *ortho* position readily convertible into iodide (Scheme 2, route 1).[52,53] 2-Iodoaniline (**1**) was diazotised by conventional means[60] and reacted in situ with pyrrolidine under basic conditions. The resulting *o*-iodoaryltriazene **2** was then converted into the corresponding boronic acid **3** by a lithiation/borylation sequence involving *n*-butyllithium and trimethylborate followed by hydrolytic workup. Suzuki–Miyaura coupling[61] of *o*-triazenylboronic acid **3** with *p*-diiodobenzene (conditions: $[PdCl_2(MeCN)_2]$, tBu_3P, K_2CO_3, dioxane/water) afforded 2,2″-bis(triazenyl)terphenyl (**4**) that was converted into 2,2″-DITP in good yield by a subsequent heating with excess of methyliodide. The complete sequence was performed in 42% overall yield.

Concerning the first step of the second route (Scheme 2, route 2), we decided to explore the protection of the amino group of the starting material **1**, to avoid any solubility and reactivity issues in the subsequent Suzuki–Miyaura cross coupling. The *tert*-Butylcarbamoyl (Boc) group was chosen as a protecting group (it is one of the most useful known protecting groups for amines).[62] The use of the non-nucleo-

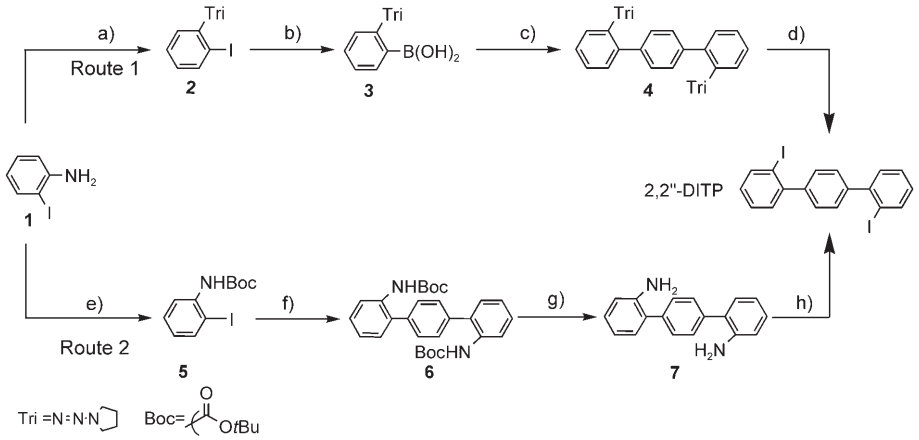

Scheme 2. Synthesis of 2,2′-DITP a) 1. $NaNO_2$, AcOH/HCl, 0°C; 2. C_4H_9N/KOH, H_2O, 0°C (95%); b) 1. *n*BuLi, Et_2O, −78°C; 2. $B(OMe)_3$, −78°C→RT; 3. H_2O/NH_4Cl (77%); c) 1,4-$C_6H_4I_2$, K_2CO_3, $[PdCl_2(MeCN)_2]$, tBu_3P, dioxane/H_2O, 80°C (89%); d) MeI, 120°C (64%); e) 1. NaHMDS, THF, RT; 2. Boc_2O (84%); f) 1,4-$C_6H_4(B(OH)_2)_2$, $[PdCl_2(dppf)]$, Na_2CO_3, DMF/H_2O, 90°C (91%); g) TFA, CH_2Cl_2, 0°C→RT (99%); h) 1. $NaNO_2$, H_2O/HCl, 0°C; 2. KI/H_2O, 0°C→60°C (63%).

philic, strong base sodium hexamethyldisilazane (NaHMDS)[63] prior the addition of the di-*tert*-butyldicarbonate (Boc_2O) leads cleanly to the corresponding *tert*-butyl-carbamoylated derivative **5**. Reaction of **5** with 1,4-phenylenebisboronic acid under Suzuki–Miyaura cross-coupling conditions with $[Pd^{II}Cl_2(dppf)]/CH_2Cl_2$ (dppf = 1,1′-bis(diphenylphosphino)ferrocene) as the catalyst and sodium carbonate as the base in a mixture of *N*,*N*-dimethylformamide and water (3:1) led to the terphenyl **6** in good yield.[64] Deprotection of the amino groups was performed under acidic conditions and diamino derivative **7** was quantitatively obtained. Although the conversion of the 2-aminobiphenyl in 2-iodobiphenyl is an easy and high-yielding reaction,[65] it was more difficult in our case to perform the Sandmeyer reaction with two free amine units instead of one. Indeed, only a few examples are reported in the literature for the concomitant conversion of two amino groups into iodine through a double Sandmeyer reaction. These reactions remain unclear and are difficult to reproduce; the resulting diiodides are mostly obtained in low yields.[4,59,66–68] The target 2,2′-DITP was obtained in 63% yield by using a tenfold excess of KI as described by Holmes and co-workers.[9] In the solid state (Figure 1), the two iodophenyl rings

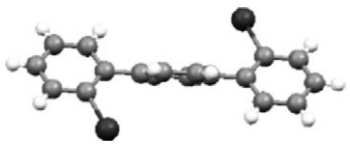

Figure 1. Crystal structure from single-crystal X-ray data of 2,2′-DITP.

of 2,2′-DITP lie on each side of the central phenyl ring (in *trans* positions to one another) with angles of around 54°.

This second sequence (Scheme 2, route 2) was satisfactorily performed with an overall yield of 48%. This new route is simple, can be performed under mild conditions, is highly adaptable, and is efficient for the preparation of 2,2′-DITP at the multigram scale.

Synthesis of substituted 2,2′-DITPs—2,2′-DITP(iPr)$_2$ and 2,2′-DITP(oct)$_2$: Two other terphenyl derivatives substituted with isopropyl (2,2′-DITP-(*i*Pr)$_2$) or octyl groups (2,2′-DITP(oct)$_2$) in the *meta* positions of the biphenyl linkage were prepared by following route 1 as previously reported.[53] However, as routes 1 and 2 involved the same *para*-alkyl-substituted starting iodoaniline it was evident that route 2 might also be used (Scheme 3).

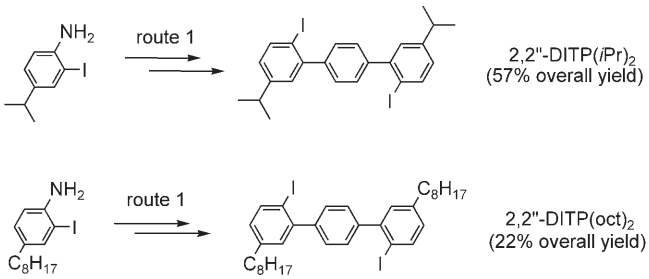

Scheme 3. Synthesis of substituted 2,2′-DITP(*i*Pr)$_2$ and 2,2′-DITP(oct)$_2$.

Synthesis of DSF-IFs: With the three terphenyl 2,2′-DITPs in hand, the lithium–iodine exchange with *n*-butyllithium in THF at low temperature followed by quenching with fluorenone gave the corresponding diols **8**–**10**, which were finally heated to reflux in acidic conditions to yield the corresponding DSF-IFs (Scheme 4).[53]

The moderate yields obtained in the lithium–halogen exchange reaction may be partially explained by the systematic formation of a byproduct identified by single-crystal X-ray diffraction as the monofluorenol **11** (Figure 2). This phenomenon has already been observed by Huang and co-workers in investigations of related compounds.[69] Depending on the conditions, this monocoupling derivative may be formed in moderate (20%) to high yield (50%).

Physicochemical properties of DSF-IF derivatives: As DSF-IFs combine 9,9′-SBF and IF frameworks, it was of great interest to compare their physicochemical properties with these two constituent building blocks. 9,9′-SBF was prepared according to literature procedures.[65,70,71] IF was prepared in a four step synthesis, by a modified Wang procedure (see details in the Supporting Information).[72]

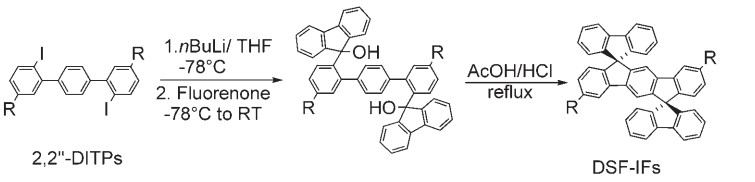

2,2''-DITP : R = H
2,2''-DITP(iPr)$_2$: R = iPr
2,2''-DITP(oct)$_2$: R = nOct

8 : R = H (56%)
9 : R = iPr (68%)
10 : R = nOct (62%)

DSF-IF : R = H (76%)
DSF-IF(iPr)$_2$: R = iPr (91%)
DSF-IF(oct)$_2$: R = nOct (83%)

Scheme 4. Synthesis of DSF-IFs.

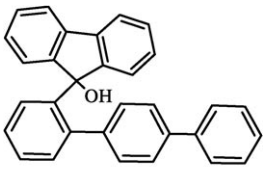

11

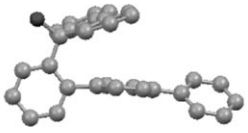

Figure 2. Crystal structure from single-crystal X-ray data of the byproduct **11** (hydrogen atoms have been omitted for clarity).

Structural properties: The DSF-IFs are dispiro molecules with a linear antarafacial geometry.[69] Single crystals of DSF-IF(iPr)$_2$ were obtained by slow diffusion of hexane into a solution of the sample in $CDCl_3$ and were analysed by X-ray diffraction in order to elucidate its molecular structure and bulk-packing characteristics (Figures 3 and 4).

The angles between the plane of indenofluorenyl moieties (through the central phenyl ring) and that of fluorenyl moieties (through the central cyclopentane ring) are 89.3 and 89°, which indicates that the fluorene rings are almost perfectly orthogonally linked through the spiro carbon. It also indicates that no additional deformation on these dispiro compounds is observed when comparing with a simple spirobifluorene X-ray structure.[57,73,74] The indenofluorenyl moiety is almost perfectly flat with only two distortions on each side, probably caused by the two isopropyl substituents.

As indicated in the crystal packing diagram of DSF-IF(iPr)$_2$ presented in Figure 4, the fluorene rings lie on each side and in the top and bottom faces of the indenofluorene plane efficiently suppressing any interchromophore interactions. The plane-to-plane distance between two indenofluorene moieties was calculated to be 5.43 Å. These structural features may reduce the excimer formation in solid film as already observed for similar structures.[75,76]

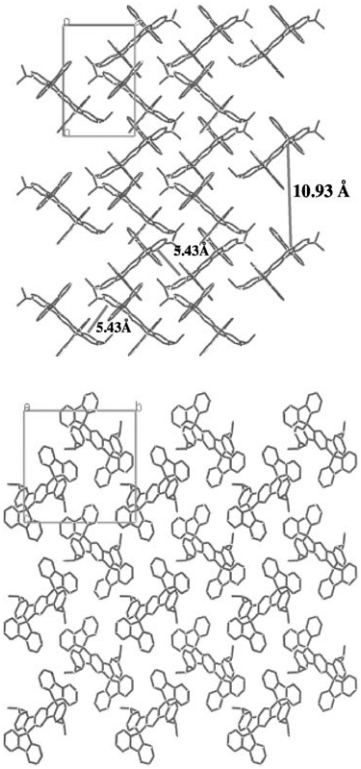

Figure 4. Crystal packing diagram of DSF-IF(iPr)$_2$. Top: along the c stacking axis. Bottom: along the a stacking axis. The co-crystallised solvent ($CDCl_3$) and the hydrogen atoms have been omitted for clarity.

Thermal properties of DSF-IF derivatives: Thermal properties were examined using thermogravimetric (TGA) and differential scanning calorimetry (DSC) analyses. The glass transition (T_g), melting transition (T_m), crystallisation (T_c) and decomposition (T_d) temperatures are summarised in Table 1. The T_d is defined as the temperature at which 5% loss occurs during heating.[51] As shown by the TGA curves presented in Figure 5a, the three DSF-IF were highly stable as they only started to decompose around 360°C for DSF-IF and DSF-IF(oct)$_2$ and around 380°C for DSF-IF(iPr)$_2$. For com-

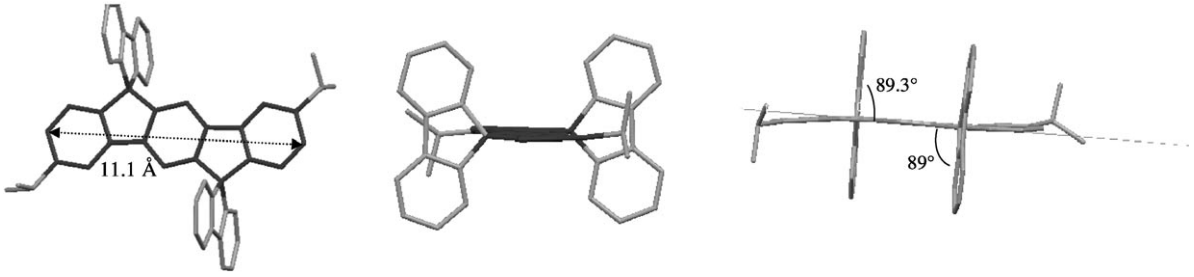

Figure 3. Crystal structure from single-crystal X-ray data of DSF-IF(iPr)$_2$ (hydrogen atoms have been omitted for clarity).

Table 1. Thermal properties of the DSF-IFs, IF and SBF [°C].[a]

	T_d[b]	T_g[c]	T_c[d]	T_m[e]
DSF-IF	355	n.o.	n.o.	n.o.
DSF-IF(iPr)$_2$	382	n.o.	n.o.	n.o.
DSF-IF(oct)$_2$	366	88	156	237
IF	200	n.d.	n.d.	n.o.
SBF	204	n.d.	n.d.	204

[a] n.d.: not determined, n.o.: not observed. [b] T_d: decomposition temperature (5% loss). [c] Tg: glass transition temperature, determined by DSC in second heating cycle. [d] T_c: crystallisation transition temperature, determined by DSC in second heating cycle. [e] T_m: melting point, determined by DSC in first heating cycle and melting point apparatus.

parison, SBF[51] and IF,[3,48,77] which have been widely used as efficient building blocks within materials for OLEDs, both start to decompose around 200°C. Thus, the higher thermal stability of the new di-spiro DSF-IFs building blocks appears to be promising for incorporation as central core of polymers or oligomers. This stability may be due to the presence of their rigid spiro-fused orthogonal bifluorene linkages, as such spiro-configuration benefit has already been described in the literature.[78–81]

Figure 5b–d show the DSC heating curves of the three DSF-IFs. In the case of DSF-IF(oct)$_2$ (Figure 5d) an endothermic peak at 237°C corresponding to the melting transition (T_m) appeared during the first run. After cooling the sample down, a glass transition temperature T_g around 88°C was observed during the second run. Further heating above the T_g resulted in the appearance of an exothermic peak (156°C) due to crystallisation and finally the melting transition again. A completely different behaviour was observed in the cases of DSF-IF (Figure 5b) and DSF-IF(iPr)$_2$ (Figure 5c). From room temperature to 300°C no significant phase transition (including T_g) was detected neither for DSF-IF nor for DSF-IF(iPr)$_2$. This phenomenon has been already observed for similar bulky structures such as spirofluorene–anthracene derivatives.[3] Such thermal behaviour is of importance to improve the lifetime of OLEDs.[2] Thus, in term of thermal properties, DSF-IF and DSF-IF(iPr)$_2$ are promising for practical use in OLEDs.

Electrochemical properties of DSF-IF derivatives—anodic behaviour: DSF-IF oxidation (Figure 6A and B) occurs along two processes which have maxima at E^1 (1.47 V) and E^2 (1.95 V). The E^1 and E^2 potential values are similar for DSF-IF(oct)$_2$ and DSF-IF(iPr)$_2$ (Table 2). This shows that the presence of alkyl groups on the indenofluorenyl moieties of DSF-IFs has only a weak influence on the oxidation potential. The donor inductive effect leads to an E^1 shift of −30 mV for octyl and −100 mV for isopropyl groups. For the three DSF-IFs, the intensities of E^1 and E^2 waves are in a ratio of 1:4 electrons. This may correspond to a first one-electron oxidation at E^1 followed by a four-electron oxidation at E^2. It should be noted that only the E^1 wave is reversible (Figure 6A). Figure 6C and E present the CVs recorded along IF and 9,9′-SBF oxidation in a similar potential range. The anodic oxidation of IF and 9,9′-SBF occurs in

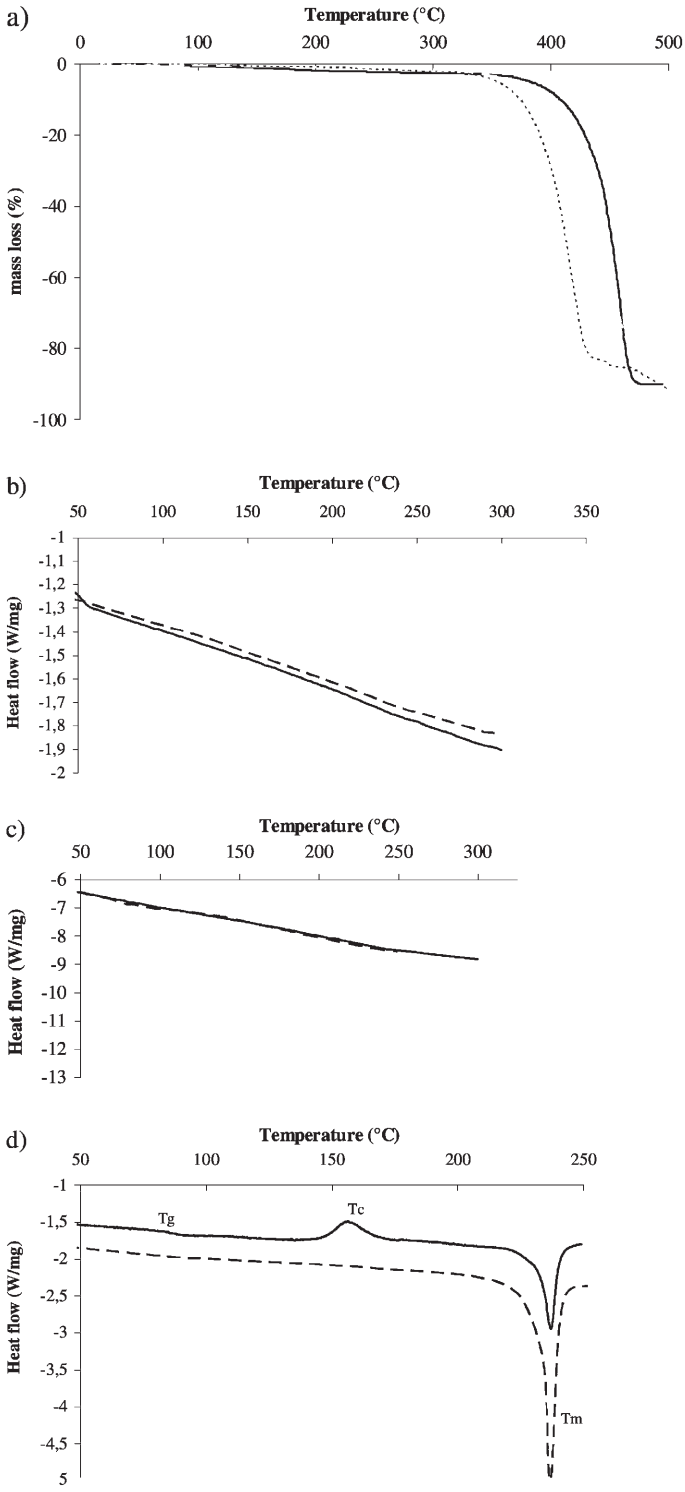

Figure 5. Thermal analysis of DSF-IFs. a) TGA curves for DSF-IF (·····); DSF-IF(iPr)$_2$ (——) and DSF-IF(oct)$_2$ (– – –). DSC curves, first run (– – –) and second run (——) for b) DSF-IF; c) DSF-IF(iPr)$_2$ and d) DSF-IF(oct)$_2$.

two waves with maxima E^1 at 1.31 and 1.69 V and E^2 at 1.81 and 1.86 V, respectively. For IF the potential shift between E^1 and E^2 is around 0.5 V whereas for 9,9′-SBF the shift between the two peaks is only 0.17 V. The intensity ratio of E^1

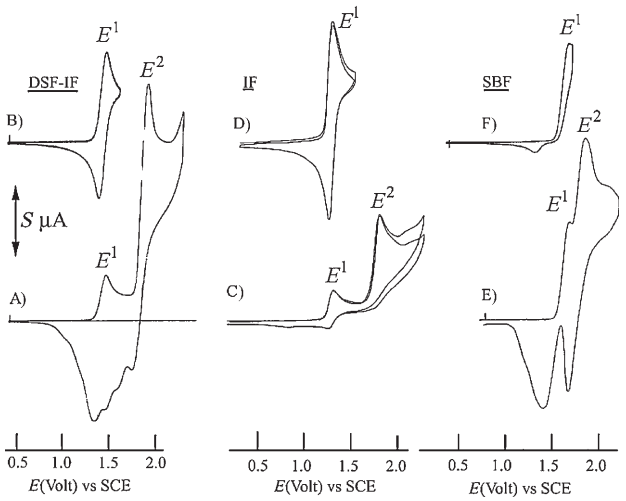

Figure 6. Cyclic voltammetry in presence of A),B) DSF-IF (3×10^{-3} M); C),D) IF (2×10^{-3} M); E),F), 9,9′-SBF (5×10^{-3} M) in CH_2Cl_2 (Bu_4NPF_6 0.2 M) for DSF-IF and 9,9′-SBF and in $CH_3CN+CH_2Cl_2$ (v/v) (Bu_4NPF_6 0.1 M) for IF; working electrode: Pt disk diameter 1 mm; sweep-rate 100 mV s^{-1}. The potential limit was 0.4–2.4 V in A; 0.4–1.7 V in B; 0.2–2.3 V in C; 0.3–1.5 V in D; 0.8–2.24 V in E; 0.37–1.7 V in F. The current scale *S* is equal to 2 in D, 4 in B, 8 in A and C and 16 in E and F.

Table 2. Electrochemical data for DSF-IFs, IF, SBF and F.

	Oxidation potential [V] vs. SCE[a]			Reduction potential [V] vs. SCE[a]	
	E^1	E^2	E^{ox}_{onset}	E^1	E^{red}_{onset}
DSF-IF	1.47	1.95	1.36	−2.32	−2.23
DSF-IF(oct)$_2$	1.44	1.99	1.30	−2.48	−2.35
DSF-IF(*i*Pr)$_2$	1.37	1.95	1.26	−2.48	−2.33
IF	1.31	1.81	1.22	−2.55	−2.41
SBF[82,83]	1.69	1.86	1.54	−2.73	−2.58
F[82,83]	1.62	–	1.48	−2.87	−2.71

[a] Obtained from CVs recorded in $CH_2Cl_2+Bu_4NPF_6$ (0.2 M) in oxidation and in DMF + Bu_4NPF_6 (0.1 M) in reduction.

and E^2 waves is 1:3 for IF and 1:1 for 9,9′-SBF. Figure 6D and F show that the wave E^1 is reversible in the case of IF and irreversible for 9,9′-SBF. As already observed for DSF-IFs, iterative cycles in the E^1 potential range of IF do not show any modification of the CV nor of the electrode surface. For 9,9′-SBF, iterative cycles leads to a slow electrodeposition process.[82,83] Finally, a comparison of the first oxidation peak of IF with the one of DSF-IF shows that IF is more easily oxidised than the indenofluorenyl unit in DSF-IF. The positive shift of 0.16 V from IF to DSF-IF oxidation may result from the electron-withdrawing effect of the spiro-linked fluorenyl units rendering the indenofluorenyl part of DSF-IF more difficult to oxidise. This might be seen as a proof of the spiroconjugation already described from a theoretical point of view in the literature.[84–91] All these observations lead us to conclude that the oxidation of DSF-IF compounds occur first through a one-electron oxidation of the indenofluorenyl part of the molecule (E^1) followed by the oxidation of the spiro-linked fluorenyl units (E^2).

Electrochemical properties of DSF-IF derivatives—cathodic behaviour: The cathodic behaviour of DSF-IF(oct)$_2$ is presented in Figure 7 together with the reduction of IF, F and 9,9′-SBF. In DMF, the DSF-IFs present a reversible reduction wave around −2.4 V (see E^1 values reported in Table 2). As expected, the inductive donor effect of the alkyl groups in DSF-IF(oct)$_2$ and DSF-IF(*i*Pr)$_2$ leads to a shift of E^1 towards more negative potentials relative to DSF-IF.

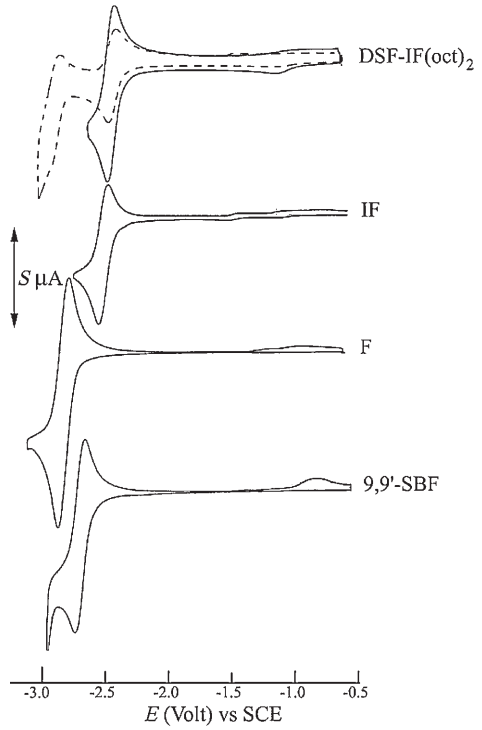

Figure 7. Cyclic voltammetry of DSF-IF(oct)$_2$ (5.78×10^{-4} M), IF (2.91×10^{-3} M), F (6.32×10^{-3} M) and 9,9′-SBF (2.4×10^{-3} M) in DMF (Bu_4NPF_6 0.1 M), working electrode: Pt disk diameter 1 mm, sweep-rate 100 mV s^{-1}. The potential limit was −0.58 V to −2.6 V for DSF-IF(oct)$_2$; −2.72 V for IF; −3.1 for F and −2.94 V for 9,9′-SBF. The current scale *S* is equal to 0.4 (——) and 0.8 (-----) for DSF-IF(oct)$_2$; 4 for IF and 9,9′-SBF and 8 for F.

IF reduction ($E^1=-2.55$ V) is slightly more difficult than that of DSF-IFs one. As already observed in the oxidation process, the spiro-linked fluorenyl groups have an electron-withdrawing effect on the indenofluorenyl part of the molecules through the spiro carbon atoms. DSF-IFs exhibit a second, quasi-reversible, reduction wave at more negative potentials close to the F and 9,9′-SBF reduction potentials (see the broken line of DSF-IF(oct)$_2$ reduction). This second reduction wave leads to the reduction of the spiro-linked fluorenyl units of the DSFIFs.

Theoretical calculations[92] are consistent with the electrochemical measurements pointing to an indeno-based primary oxidation and reduction in DSF-IFs, as shown by the calculated nature of the frontier molecular orbitals of DSF-

IF in Figure 8. Indeed, we note the indenofluorenyl character of the HOMO and LUMO and the spirofluorenyl character of the two pairs of quasi-degenerate LUMO+1, LUMO+2 and HOMO−1, HOMO−2.

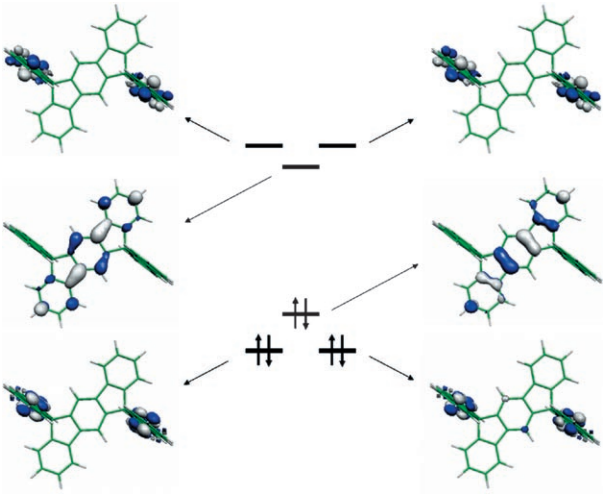

Figure 8. Sketch of DSF-IF frontier molecular orbitals from Gaussian03 B3LYP/6–31G* calculations.[92–94]

Electrochemical and optical band gap: Following the work of Jenekhe,[95] we did an experimental estimation of the electron affinity (EA) or lowest unoccupied molecular orbital (LUMO) and of the ionisation potential (IP) or highest occupied molecular orbital (HOMO) from the redox data (Table 3). The LUMO level was calculated from: LUMO (eV) $= -[E^{red}_{onset}$ (vs SCE) $+4.4]$ and the HOMO level from: HOMO (eV) $= -[E^{ox}_{onset}$ (vs SCE) $+4.4]$, based on an SCE energy level of 4.4 eV relative to the vacuum. The electrochemical gap ΔE^{el} obtained as $E^{ox}_{onset} - E^{red}_{onset}$ (in eV) was also compared to the optical band gap calculated from the absorption edge of the UV/Vis absorption spectra using the formula ΔE^{opt} (eV) $= hc/\lambda$.

The calculated band gaps from electrochemical data of DSF-IFs are consistent with the measured optical band gaps with only a small deviation (0.2 eV or less). These values are also qualitatively consistent with the theoretical values obtained with DFT calculations: although the HOMOs and especially the LUMOs energies are overestimated by the DFT method (ca. 0.1–0.4 and 0.9–1 eV respectively), the experimental trend in the frontier molecular orbital energy and associated band gap is well reproduced theoretically. The DSF-IFs band gap appears to be wide (3.5/3.6 eV) with a HOMO level around −5.7 eV and the LUMO level around −2.1 eV. SBF and F have a larger band gap (larger than 4 eV) with a deeper HOMO and a higher LUMO. As a consequence, the DSF-IFs compounds are interesting in this respect, for electroluminescent devices, since their energy level better fit the cathode and anode work function (see Figure 13 in a later section).

Anodic electrodeposition—synthesis of electroactive polymers: The first oxidation of DSF-IFs involves the indenofluorenyl part of the molecules in a one-electron process (vide supra), whereas the second oxidation occurs on the two spiro-linked fluorenyl units. This second process occurs in a potential range slightly more positive than the oxidation potential of SBF and F oxidation (Table 2). These two compounds are known to undergo electropolymerisation processes[82,83,97–99] and DSF-IFs present the same behaviour. Indeed, recurrent sweeps between 0.5 and E^2 lead to gradual modification of the CVs and to the modification of the electrode surface by an insoluble transparent deposit. The deposits derived from DSF-IFs are three-dimensional compounds with high electrochemical stability and interesting electrochromic behaviour (see Figure 9).

Oxidation on transparent ITO-glass electrodes, allowed the observation of the intense blue DSF-IF radical cations generated at E^1 and the pink radical cations generated at E^2. The observation of these colourations allows us to assert that DSF-IF polymerisation occurs in good yield as one observed no diffusion of coloured species in solution at the vicinity of the electrode along the electrodeposition process. Upon reduction at 0.5 V, the deposit became instantaneously transparent.

Coulometric measurements recorded along DSF-IF oxidation (see details in the Supporting Information) show that the p-doping level, called *m* in this work, of the spiro-linked fluorene units is between 0.7 and 1 electron. This value is equivalent to the one of poly(9,9′-SBF) but higher than the one poly(F), that is, 0.3 electrons.

The three poly(DSF-IFs) present a similar electrochemical behaviour in terms of onset oxidation potential, potential range of stability and p-doping level. This shows that the substitution of the indenofluorenyl

Table 3. Molecular frontier orbital energy and HOMO/LUMO gaps of DSF-IFs, IF, SBF and F from electrochemical, optical and theoretical data.

	HOMO [eV][a]	LUMO [eV][b]	HOMO [eV][c]	LUMO [eV][c]	ΔE^{el} [eV][d]	ΔE^{opt} [eV][e]	ΔE^{calc} [eV][f]
	from redox data		from calculations				
DSF-IF	−5.76	−2.17	−5.41	−1.23	3.59	3.51	4.18
DSF-IF(oct)$_2$	−5.70	−2.05	–	–	3.65	3.47	–
DSF-IF(*i*Pr)$_2$	−5.66	−2.07	−5.35	−1.19	3.59	3.44	4.16
IF	−5.62	−1.99	−5.43	−1.13	3.63	3.61	4.30
SBF	−5.94	−1.82	−5.69	−0.84	4.12	3.91	4.85
F	−5.88	−1.69	−5.81	−0.77	4.19	3.97	5.04

[a] Calculated from the onset oxidation potential. [b] Calculated from the onset reduction potential. [c] Gaussian 03 B3LYP/6–31G* calculation:[92,94] a SCRF solvation model[96]was applied to the optimised geometry of each model using dichloromethane and acetonitrile for the determination of the HOMO and LUMO energy respectively. [d] Calculated as $\Delta E^{el} = E^{ox}_{onset} - E^{red}_{onset}$. [e] Calculated from the absorption edge of the absorption spectrum using $\Delta E^{opt} = hc/\lambda$. [f] $\Delta E^{calc} = |\text{HOMO} - \text{LUMO}|$ from theoretical calculations.

part of the molecule by an alkyl group does not influence the p-doping process of the polyfluorenyl chains. Figure 9B–D present the anodic behaviour of poly(DSF-IF) deposits.

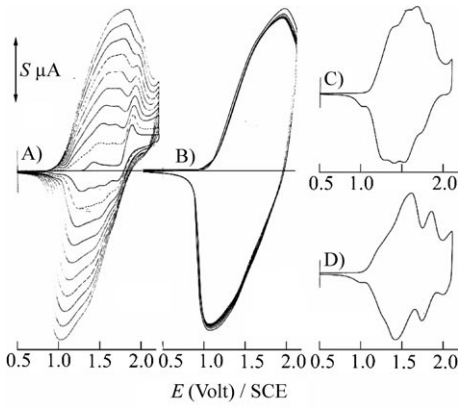

Figure 9. Cyclic voltammetry in CH_2Cl_2 (Bu_4NPF_6 0.2 M). A) DSF-IF (3×10^{-3} M), ten sweeps between 0.5 and 2.22 V, working electrode: Pt disk diameter 1 mm. B)–D) working electrode: Pt disk diameter 1 mm modified by a deposit of poly(DSF-IF). For B, the electrodeposition was performed along the CVs recorded in A; for C and D the electrodeposition was performed by oxidation of a 3×10^{-3} M solution of DSF-IF in CH_2Cl_2 (Bu_4NPF_6 0.2 M) at fixed potential: 1.9 V for C and 2.3 V for D with Q_t, the amount of charge for the formation, equal to 2×10^{-4} C. The potential limit was 0.24 to 2.1 V in B and 0.5 to 2.1 V in C and D. The current scale S is equal to 40 in A and B and to 16 in C and D. Sweep-rate: 100 mV s^{-1}.

In B, the deposit was obtained along the CVs recorded Figure 9A. The onset oxidation potential of the deposit is at 0.94 V, negatively shifted of 420 mV when compared to the E^{ox}_{onset} of DSF-IF signing an extension of the conjugation length in the polymer. The deposit is electrochemically stable (reversibility of the p-doping process higher than 95%) in a rather large potential range (up to more than 2 V). CVs reported Figure 9C,D were recorded for thin deposits of poly(DSF-IF) prepared at different potentials ($E=1.9$ and 2.3 V, see the Supporting Information). For the deposit prepared at the lowest potential (Figure 9C), the first wave is associated with the oxidation of the indenofluorenyl part of the polymer and is followed by three other waves that might be attributed to the different oxidation levels of the polyfluorenyl chains. For the deposit prepared at higher potential (Figure 9D), the oxidation of the indenofluorenyl part appears as a shoulder before the two oxidation waves of the polyfluorenyl chains. Coulometric measurements were also performed along poly(DSF-IF) p-doping process between 0.5 and 2.1 V and show that the p-doping level, called m' in this work, of the spiro-linked fluorene units is between 1 and 1.7. The higher m' values, relative to the m values, are due to the higher potential reached along the p-doping process. The m' values show the high-energy storage potential of the poly(DSF-IF).

Electrochromic properties of these polymers were observed when switching their oxidation state from their neutral to their p-doped level. The deposit changes colour from transparent to purple with a short switching time and a good stability of the switch measured along chronoamperometric exploration. As the current keeps more than 95% of its initial value (after 1000 cycles), these polymers possess highly interesting electrochromic properties.[100]

In terms of mechanism, and keeping in mind the electropolymerisation process of F and 9,9′-SBF already described in literature,[99] we expected that the polymerisation of DSF-IF begins by the one-electron oxidation of the indenofluorenyl part of the molecule at E^1, followed by the oxidation of the spiro-linked fluorenyl units at E^2. The cation radical of these units are quickly involved in dimerisation processes. The formation of the C–C bond leads to new dihydrodimer–dications that lose protons to form the final dimers. The electrogenerated dimers are easier to oxidise than the starting monomer and give new dimer radical cations at the level of the monomer oxidation potential. Then, these dimer radical cations will repeat the coupling step to form trimers, tetramers and so forth. The reduction of the deposit at 0.5 V lead to the charge neutralisation and the formation of the neutral poly(DSF-IFs) (Scheme 5). This scheme, which is an ideal representation of the polymer network, is however informative as it shows that the aromatic polyfluorenyl chains are well organised in parallel wires, with no evident interchain communication between one another due to the indenofluorenyl groups.

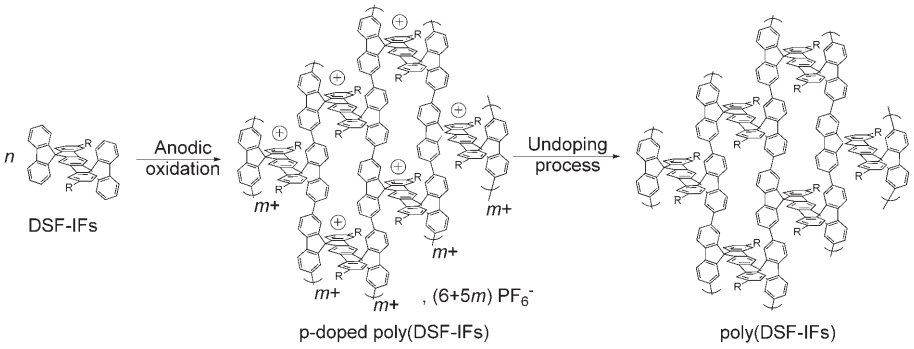

Scheme 5. Schematic representation of DSF-IFs electrodeposition.

Optical properties of DSF-IF derivatives

UV/Vis absorption spectra of the DSF-IFs: The UV/Vis absorption of DSF-IFs were first studied and compared with the UV/Vis absorption of F, SBF and IF (Table 4, Figure 10, top). For solubility purposes, these compounds were all studied in solution in CH_2Cl_2. F and SBF have similar absorption

Table 4. Photophysical properties

	λ_{Abs} [nm][a]	λ_{Exc} [nm]	λ_{Em} [nm][a,b]	ϕ_{sol} [%][c]
DSF-IF	231, 254, 300, 311, 330, 337, 345	344	347, 356, 366	62
DSF-IF(iPr)$_2$	231, 254, 300, 311, 333, 340, 348	348	351, 359, 370	66
DSF-IF(oct)$_2$	228, 254, 301, 312, 334, 341, 349	348	351, 359, 370	66
IF	228, 235, 289, 302, 319, 328, 334	334	339, 347, 356	61
SBF	229, 252, 297, 309	309	312, 323	20

[a] Measured in dichloromethane. [b] Measured in cyclohexane for all compounds except for IF (decalin). [c] The relative quantum yield was measured with reference to quinine sulphate in 1 N H_2SO_4 ($\phi = 0.546$).

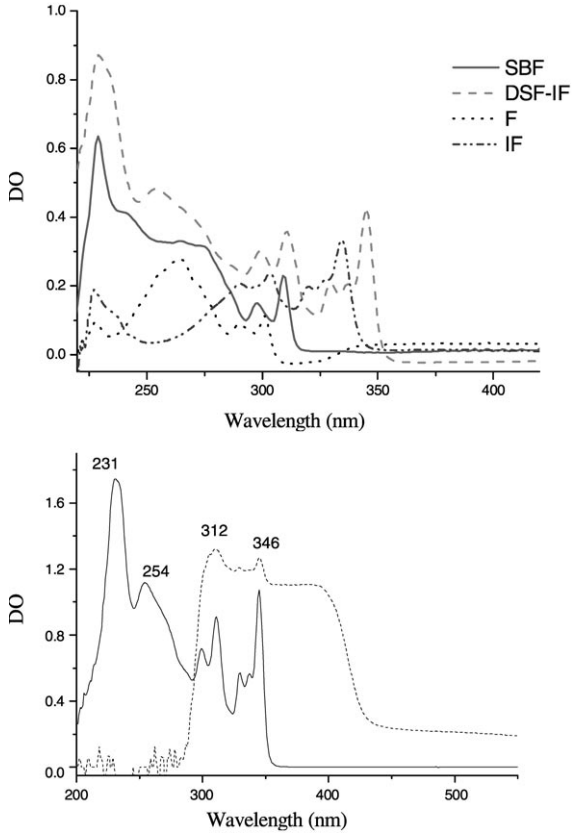

Figure 10. Top: UV/Vis spectra of DSF-IF (-----), F (•••••), SBF (——) and IF (–•–•) in solution in CH_2Cl_2 (10^{-5} M). Bottom: UV/Vis spectra of DSF-IF in solution in CH_2Cl_2 (——), poly-DSF-IF deposited on an ITO electrode plunged in CH_2Cl_2 (-----).

spectra, displaying two sharp bands (290 and 301 for F, 297 and 309 nm for SBF) in addition to a broad one around 250–265 nm. The electronic spectra of DSF-IFs present absorption bands around 230, 254, 300, 310 as for F and SBF and three additional bands around 330–335, 335–340 and 345–350 nm. For DSF-IF we precisely observed these three bands at 330, 337 and 345 nm, which are in accordance with the absorption bands of IF at 319, 328 and 334 nm,[72] but bathochromically shifted by about 10 nm. This shift may be assigned to the influence of the spiro-linked F rings on the IF moieties. This effect may arise from the interactions between the two orthogonally linked π systems, that is, spiro-conjugation, as already observed with CV.

UV/Vis absorption spectra of the polymers: Poly(DSF-IF) spectrum exhibits a large absorption band between 300 and 350 nm due the more extended conjugation than in the DSF-IF monomer (Figure 10, bottom). Such a large band was also observed as the main absorption band in poly(SBF).[82,83] We also observed two sharp peaks at 312 and 346 nm. These absorptions fit well with those of DSF-IF (Figure 10, top) and confirm the presence of DSF-IF patterns in the polymeric network.

Emission spectra: The photoluminescence of DSF-IFs was studied in cyclohexane and compared with SBF and IF in order to evaluate the efficiency of these molecules as key structures for further OLED applications (Figure 11 and Table 4). The central building block IF exhibits two main emissions ($\lambda_{exc} = 334$ nm) with maxima at 339 and 356 nm (Figure 11). DSF-IF after excitation at 344 nm shows two similar emissions at 347 and 366 nm. This 10 nm shift, already observed in the UV/Vis absorption (Figure 10, top) may be attributed to the interaction between the F rings and the central IF ring through the spiro-carbon. DSF-IF(iPr)$_2$ and DSF-IF(oct)$_2$ exhibit the same behaviour with emission at 351 and 370 nm. The small Stokes shift observed for DSF-IFs is consistent with the rigidity observed in the solid state structure. ϕ_{sol} was determined by using standard procedures with quinine sulphate dihydrate as reference.[72] IF exhibits a quantum yield of 61%, slightly lower than the results reported by Wang.[72] The three DSF-IFs appear to be highly efficiently fluorescent with high quantum yields of around 65%.

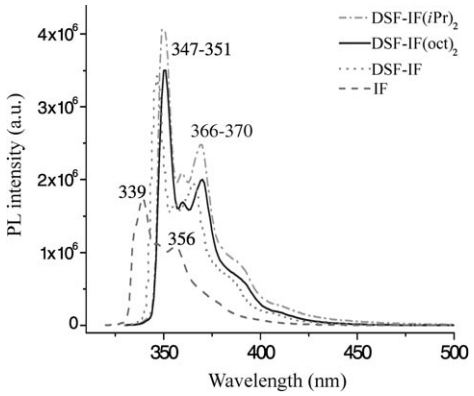

Figure 11. Emission spectra: 6×10^{-7} M solutions of DSF-IF (•••••), DSF-IF(iPr)$_2$ (–•–•) DSF-IF(oct)$_2$ (——) in cyclohexane, IF (-----) in decalin.

Organic light-emitting diodes (OLEDs) using DSF-IFs as the emitting layer: As the DSF-IF core may be interesting

as a new building block for electroluminescent devices, it seemed of great interest to study its behaviour in OLEDs. DSF-IF, DSF-IF(iPr)$_2$ and DSF-IF(oct)$_2$ exhibited similar electroluminescence properties therefore only results on DSF-IF(iPr)$_2$ are presented. Basic OLED structures with ITO as the anode, poly(3,4-ethylene dioxythiophene) doped with poly(styrene sulfonate): PEDOT/PSS as the hole injecting layer (HIL), DSF-IF(iPr)$_2$ as the emitting layer (EML) and Ca as the cathode were first fabricated and characterised (Figure 12a). The associated band energy diagram of

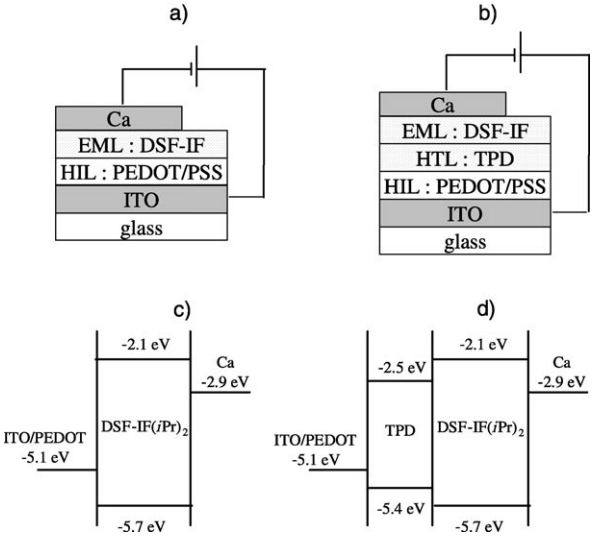

Figure 12. a), b) Structures of the investigated OLEDs. HIL, HTL and EML correspond to the hole-injecting layer, the hole-transport layer and the emitting layer, respectively. c), d) Schematic representation (before contact) of the energetic structure associated with the investigated devices.

that structure is presented in Figure 12c. The LUMO of DSF-IF(iPr)$_2$ is very low (−2.1 eV), therefore a cathode with a low work function needs to be used in order to enable charge injection into the DSF-IF(iPr)$_2$ layer. Calcium seemed the most appropriate available metal for that purpose with a work function of −2.9 eV. LiF/Al was also tested but resulted in lower efficiency OLEDs.

The normalised electroluminescence spectrum recorded for ITO/PEDOT/DSF-IF(iPr)$_2$/Ca devices (Figure 13) exhibits two main emission peaks in the blue region at 399 and 416 nm. Two other contributions are found at 483 and 587 nm. The chromatic coordinates calculated from the electroluminescence spectrum in the CIE 1964 chromaticity diagram are (0.21; 0.16). These coordinates correspond to a blue colour as can be seen on Figure 13.

Current-density–voltage–luminance characteristics of the ITO/PEDOT/DSF-IF(iPr)$_2$/Ca OLEDs are presented in Figure 14 (top). The turn on voltage appears around 7 V. The luminance of the device reaches 200 Cd m^{-2} at 15 V and for a current density of 22 mA cm^{-2}. In terms of efficiency, the devices reach 0.9 Cd A^{-1} and 0.19 Lm W^{-1} at 200 Cd m^{-2}

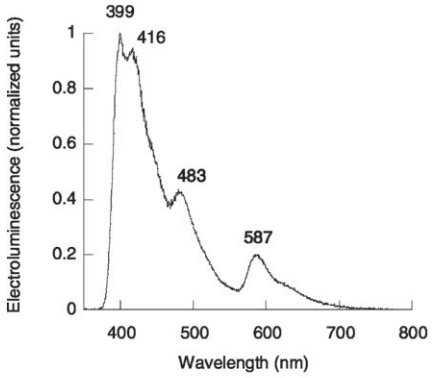

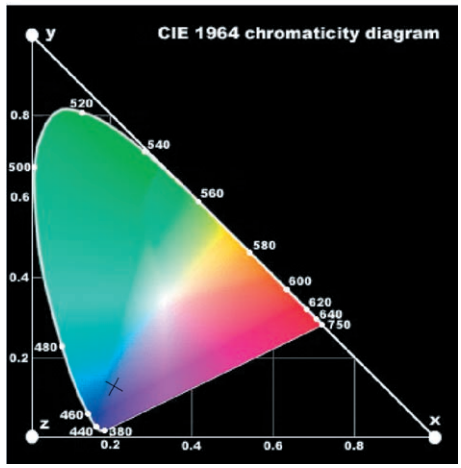

Figure 13. Electroluminescence spectrum of ITO/PEDOT/DSF-IF(iPr)$_2$/Ca device with the corresponding colour placed on the CIE 1964 chromaticity diagram.

(Figure 14, bottom), which is promising for single-layer blue OLEDs.

To improve the performances of the DSF-IF(iPr)$_2$-based OLEDs a hole transport layer (HTL), *N*,*N*′-diphenyl-*N*,*N*′-bis(3-methylphenyl)-[1,1′-biphenyl]-4,4′-diamine (TPD) was inserted between the anode and the emitting layer (Figure 12b and d).[101] The HOMO energy level of TPD lies between those of PEDOT and DSF-IF(iPr)$_2$. This should result in an easier hole injection into the DSF-IF(iPr)$_2$ layer. However the comparison of the voltage–luminance characteristics of the OLEDs with and without TPD (Figure 15) reveal poorer performances of the TPD/DSF-IF(iPr)$_2$-based device both in terms of luminance and efficiency. The TPD-based OLEDs reach a maximum efficiency of 0.4 Cd A^{-1} versus 0.9 Cd A^{-1} for the single-layer DSF-IF(iPr)$_2$-only device (vide supra). Furthermore the threshold voltage is slightly increased. This can be due to the additional TPD layer, which causes a global increase of the organic layer thickness and results in a higher turn-on voltage. Moreover, the LUMO level of TPD (−2.5 eV) lies below that of DSF-IF(iPr)$_2$ (−2.1 eV). As a consequence, when electrons are injected into the DSF-IF(iPr)$_2$ layer they are not confined within that layer as there is no energetic barrier to cross at the DSF-IF(iPr)$_2$/TPD interface. The use of an electron

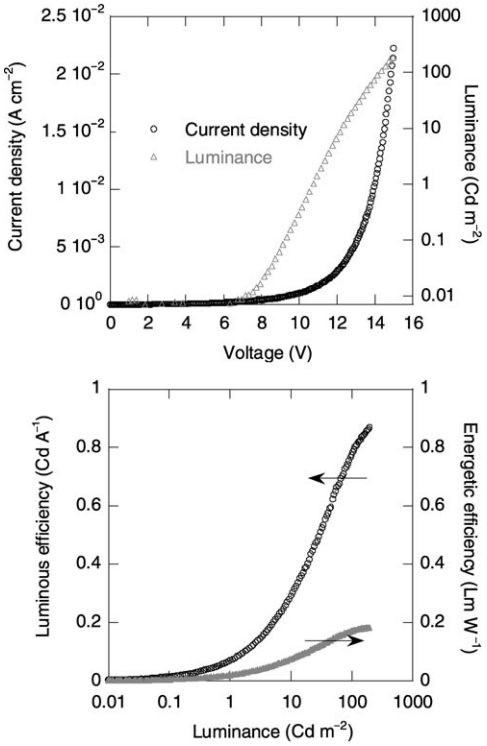

Figure 14. Top: I-V-L characteristics. Bottom: luminous and energetic efficiencies of an ITO/PEDOT/DSF-IF(iPr)$_2$ (30 nm)/Ca OLED.

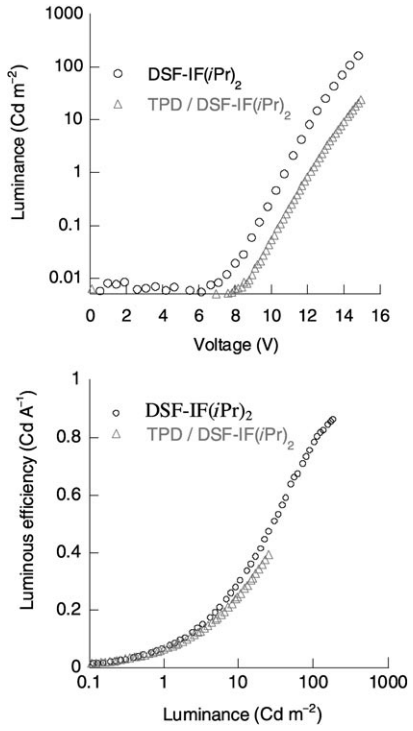

Figure 15. Top: Luminance–voltage characteristics. Bottom: luminous efficiency of OLEDs with the following structures: ITO/PEDOT/DSF-IF(iPr)$_2$ (30 nm)/Ca and ITO/PEDOT/TPD (20 nm)DSF-IF(iPr)$_2$ (30 nm)/Ca.

blocking layer with a LUMO level significantly above −2.1 eV would improve the confinement of electrons. Similarly, holes are not confined within the DSFIF(iPr)$_2$ layer. Therefore, some charge carriers (electrons and holes) can cross the emitting layer without radiative recombination. This causes a decrease of efficiency.

To enhance injection electrons and block holes, Alq3 is often inserted between the emitting layer and the cathode. A ITO/PEDOT/TPD/DSF-IF(iPr)$_2$/Alq3/Ca device has been made but its electroluminescence spectra showed a contribution of Alq3. Indeed, the LUMO level of Alq3 (−3.1 eV) lies below that of DSF-IF(iPr)$_2$ (−2.1 eV) as well as below the work-function of Ca (−2.9 eV). It means that electrons are confined in the Alq3 layer instead of in the emitting layer. Moreover, as the HOMO level of Alq3 (−5.6 eV) lies slightly above that of DSF-IF(iPr)$_2$ (−5.7 eV), no hole blocking effect can be observed. This confirms that Alq3 is not a suitable material to enhance both electron injection and hole-blocking processes in those systems. Similarly, Wu and co-workers did not observe any hole blocking in PPV derivatives.[102] The use of a electron and/or hole-blocking layers able to confine charge carriers in the DSF-IF(iPr)$_2$ layer appears essential for multilayer devices.

Conclusion

In summary we have synthesised a series of new luminophores combining one indenofluorenyl unit and two spiro-linked fluorenyl units. These molecules, called DSF-IFs, have been prepared by short efficient syntheses through a key di-iodinated terphenyl intermediate (2,2″-DITP). We believe this intermediate might be of great interest for the elaboration of other dispiro compounds for organic optoelectronics. Their electrochemical behaviour has been studied and compared to their constituent building blocks, that is, IF and SBF, to evaluate their HOMO/LUMO levels and to understand their electronic properties. These results have been confirmed by DFT calculations. The thermal and photophysical properties of DSF-IFs have been estimated and appeared to be promising for OLED applications. These versatile molecules may be also polymerised through the fluorene cores, and lead to electroactive three-dimensional materials with interesting optical and electrochromic properties. The preliminary studies carried out on DSF-IFs for the OLED application led to interesting and promising properties for blue emitters. Indeed, DSF-IF(iPr)$_2$ exhibits good performances when used in a single-layer device. The efficiencies could even be further increased with the use of charge-blocking layers. Further optimisations of the devices are currently in progress and will be reported in due course.

Experimental Section

General: Commercially available reagents and solvents were used without further purification other than those detailed below. Dichloro-

methane was distilled over calcium hydride prior to use. THF and cyclohexane was distilled from sodium/benzophenone. Light petroleum refers to the fraction with b.p. 40–60 °C.

Synthesis: Reactions were stirred magnetically, unless otherwise indicated. Analytical thin-layer chromatography was carried out using aluminium-backed plates coated with Merck Kieselgel 60 GF_{254} and visualised under UV light (at 254 and/or 360 nm). Chromatography was carried out with silica 60 A CC 40–63 μm (SDS). ^1H and ^{13}C NMR spectra were recorded on Bruker 200 and 300 MHz instruments (^1H frequencies, corresponding ^{13}C frequencies are 50 and 75 MHz); chemical shifts were recorded in ppm and J values in Hz. In the ^{13}C NMR spectra, signals corresponding to CH, CH_2 or Me groups, assigned from DEPT, are noted; all others are C. The residual signals for the NMR solvents are: $CDCl_3$; 7.26 ppm for the proton and 77.00 ppm for the carbon, CD_3OD; 3.31 ppm for the proton and 49.05 ppm for the carbon, $(CD_3)_2SO$; 2.50 ppm for the proton and 39.43 ppm for the carbon. The following abbreviations have been used for the NMR assignment: s for singlet, d for doublet, t for triplet, q for quintet and m for multiplet. "br" abbreviation means that the signal is broad. High-resolution mass spectra were recorded at the CRMPO (Rennes). Substituted 2,2′′-DITPs and the corresponding DSF-IFs were prepared according literature procedures.[53] 9,9′-SBF was prepared according literature procedures.[65,70,71] IF was prepared in a four-step synthesis by a modified Wang procedure (see details in Supporting Information).[72]

(2-Iodophenyl)carbamic acid *tert*-butyl ester (5): Sodium bis(trimethylsilyl)amide (8.2 mL, 16.4 mmol) was added dropwise to a stirred solution of **1** (1.8 g, 8.2 mmol) in dry THF (7.5 mL) at room temperature under an argon atmosphere. After 25 min, di-*tert*-butyldicarbonate (1.9 g, 8.2 mmol) was added over 5 min by syringe. The reaction mixture was stirred at room temperature for 2 h. Water (50 mL) was then added, and the resulting mixture was extracted with dichloromethane (3×50 mL). The organic layer was washed with a saturated aqueous solution of sodium chloride (50 mL), dried ($MgSO_4$), and evaporated in vacuo. Purification by column chromatography on silica gel eluting with ethyl acetate/light petroleum (1:9) gave compound **5** (2.2 g, 84 %) as a yellow/orange oil. ^1H NMR (300 MHz; $CDCl_3$): $\delta=8.04$ (dd, $J=7.5$, 1.5 Hz, 1H; ArH), 7.74 (dd, $J=7.5$, 1.5 Hz, 1H; ArH), 7.31 (td, $J=7.5$, 1.5 Hz, 1H; ArH), 6.82 (s, 1H; NH), 6.76 (td, $J=7.5$, 1.5 Hz, 1H; ArH), 1.54 ppm (s, 9H; Me); ^{13}C NMR (75 MHz; $CDCl_3$): $\delta=152.5$ (C=O), 138.8 (CH), 138.77 (C), 129.1 (CH), 124.6 (CH), 120.1 (CH), 88.7 (C-I), 81 (C), 28.3 ppm (CH_3); HRMS (EI): m/z calcd for $C_{11}H_{14}INO_2$: 319.00693 $[M]^+$; found: 319.0038.

2,2′′-Di-*tert*-butylbiscarbamate[1,1′:4′,1′′] terphenyl (6): Sodium carbonate (3.3 g, 31.5 mmol) dissolved in water (7 mL) was added to a solution of *tert*-butyl (2-iodophenyl)carbamate **5** (2.7 g, 8.5 mmol), 1,4-phenylene bisboronic acid (0.5 g, 3.2 mmol) and 1,1′-bis(diphenylphosphino)ferrocene palladium(II)dichloride dichloromethane complex (0.1 g, 0.1 mmol) in DMF (22 mL) at room temperature. The Schlenk tube was degassed, and the mixture was allowed to stir at 90 °C for 12 h under an argon atmosphere. The reaction mixture was then quenched with water (100 mL) and extracted with ethyl acetate (4×50 mL). The combined organic layers were washed with a saturated aqueous solution of sodium hydrogencarbonate (50 mL), dried ($MgSO_4$) and evaporated in vacuo. Purification by column chromatography on silica gel eluting with ethyl acetate/light petroleum (1:10) afforded compound **6** (1.3 g, 91 %) as a colourless solid. M.p. 140–142 °C (acetonitrile); ^1H NMR (300 MHz; $CDCl_3$): $\delta=8.10$ (d, $J=8.3$ Hz, 2H; ArH), 7.50 (s, 4H; ArH), 7.37 (td, $J=8.3$, 1.5 Hz, 2H; ArH), 7.26 (dd, $J=8.3$, 1.5 Hz, 2H; ArH), 7.14 (td, $J=8.3$, 1.5 Hz, 2H; ArH), 6.57 (s, 2H; NH), 1.48 ppm (s, 18H; Me); ^{13}C NMR (75 MHz; $CDCl_3$): $\delta=152.9$ (C=O), 137.9 (C), 135.2 (C), 131 (C), 130.3 (CH), 129.9 (CH), 128.6 (CH), 123.4 (CH), 120.4 (CH), 80.6 (C), 28.3 ppm (Me); IR (KBr): $\tilde{\nu}=3250$ (NH), 3028, 2978, 2931, 2870, 2815, 2761, 2715, 2284, 2205, 1930, 1915, 1700 (CO), 1581, 1529, 1476, 1448, 1391, 1366, 1304, 1289, 1245, 1164, 1040, 1036, 1007 cm^{-1}; HRMS (EI): m/z calcd for $C_{28}H_{32}N_2O_4{\cdot}CO_2C_4H_8$: 360.18378 $[M-CO_2C_4H_8]^+$; found: 360.1861.

1,1′:4′,1′′-Terphenyl-2,2′′-diamine (7): Trifluoroacetic acid (17.0 mL, 229.0 mmol) was added to a solution of compound **6** (1.8 g, 3.9 mmol) in dichloromethane (200 mL) at room temperature. The reaction mixture was allowed to stir at room temperature for 4 h and was then cooled to 0 °C and carefully neutralised (pH ≈ 7–8) with a saturated aqueous solution of sodium hydrogencarbonate. The resulting mixture was extracted with dichloromethane (3×50 mL). The organic layer was dried ($MgSO_4$) and evaporated in vacuo to give compound **7** (1.1 g, 99 %) as a colourless solid. M.p. 212 °C (dichloromethane/hexane); ^1H NMR (300 MHz; $CDCl_3$): $\delta=7.55$ (s, 4H; ArH), 7.21–7.15 (m, 4H; ArH), 6.88–6.78 (m, 4H; ArH), 3.42 ppm (brs, 4H; NH); ^{13}C NMR (75 MHz; $CDCl_3$): $\delta=$ 143.5 (C), 138.3 (C), 130.4 (CH), 129.4 (CH), 128.5 (CH), 137.1 (C), 118.7 (CH), 115.6 ppm (CH); HRMS (EI): m/z calcd for $C_{18}H_{16}N_2$: 260.13135 $[M]^+$; found: 260.1327.

2,2′′-Diiodo-[1,1′:4′,1′′]terphenyl (2,2′′-DITP): Sodium nitrite (1.8 g, 26.1 mmol) dissolved in water (72 mL) and cooled at 0 °C was added sequentially over 15 min to a stirred solution of compound **7** (2.7 g, 10.4 mmol) suspended in water (135 mL) containing concentrated hydrochloric acid (38 mL) at 0 °C. The clear yellow solution was stirred for 1 h at 0 °C (solution 1). In a separate vessel, a solution of potassium iodide (17.4 g, 104.8 mmol) in water (190 mL) was cooled to 0 °C (solution 2). Solution 1 was added to solution 2 over 10 min at 0 °C and the dark red solution was stirred for a further 1 h at 0 °C. The ice bath was removed and the mixture was stirred at room temperature for 2 h and then heated to 60 °C for a further 2.5 h. The resulting mixture was stirred at room temperature overnight and extracted with dichloromethane (5×100 mL). The organic layers were washed with water, dried ($MgSO_4$) and the solvent was removed in vacuo. The red crude product was purified by column chromatography on silica gel eluting first with light petroleum and second with dichloromethane/light petroleum (1:9). After removal of the solvents, crystallisation (light petroleum) afforded compound 2,2′′-DITP (3.0 g, 63 %) as a colourless solid. M.p. 156 °C (light petroleum) (lit. [59]; m.p. 158.9 °C (ethanol)); ^1H NMR (300 MHz; $CDCl_3$): $\delta=7.98$ (d, $J=7.5$ Hz, 2H; ArH), 7.42–7.39 (m, 8H; ArH), 7.08–7.03 ppm (m, 2H; ArH); ^{13}C NMR (75 MHz; $CDCl_3$): $\delta=146.2$ (C), 143.3 (C), 139.6 (CH), 130.1 (CH), 128.84 (CH), 128.81 (CH), 128.1 (CH), 98.5 ppm (C-I); IR (KBr): $\tilde{\nu}=3060$, 3038, 1929, 1911, 1800, 1583, 1555, 1458, 1424, 1391, 1250, 1005, 999 cm^{-1}; HRMS (EI): m/z calcd for $C_{18}H_{12}I_2$: 481.90285 $[M]^+$; found: 481.9027; elemental analysis calcd (%) for $C_{18}H_{12}I_2$: C 44.8, H 2.5; found: C 44.4, H 2.5.

9-[1,1′:4′,1′′]Terphenyl-2′′-yl-9*H*-fluoren-9-ol (11): Mono alcohol derivative **11** was obtained as a byproduct during the coupling of the 9-fluorenone and 2,2′′-DITP. M.p. 123.5 °C; ^1H NMR (300 MHz; $CDCl_3$) $\delta=$ 8.51 (d, $J=7.5$ Hz, 1H; ArH), 7.64–7.11 (m, 15H; ArH), 6.97 (d, $J=$ 7.5 Hz, 1H; ArH), 6.81 (d, $J=8.3$ Hz, 2H; ArH), 6.06 (d, $J=8.3$ Hz, 2H; ArH), 2.46 ppm (brs, 1H; OH); ^{13}C NMR (75 MHz; $CDCl_3$): $\delta=150.6$, 148.8, 141.5, 141.4, 141.3, 140.6, 140.3, 140.1, 139.6, 139.4, 137.8, 131.0, 129.2, 128.8, 128.7, 127.9, 127.2, 126.9, 126.3, 124.9, 124.4, 123.5, 120.0, 119.9, 82.41 ppm; HRMS (EI): m/z calcd for $C_{31}H_{22}O$: 410.16707 $[M]^+$; found: 410.1691.

Spectroscopic studies: UV/Vis spectra were recorded using a UV/Visible spectrophotometer UVIKON XL Biotech. The optical band gap was calculated from the absorption edge of the UV/Vis absorption spectra by using the formula ΔE^{opt} (eV) $= hc/\lambda$ in which λ is the absorption edge (in m). With $h=6.6262\times10^{-34}$ J s (1 eV $=1.602\times10^{-19}$ J) and $c=2.99\times10^8$ m s^{-1}, this equation may be simplified as: ΔE^{opt} (eV) $=1237.5/\lambda$ (λ in nm). Photoluminescence spectra were recorded at room temperature with a PTI spectrofluorimeter (PTI-814 PDS, MD 5020, LPS 220B) using a xenon lamp. Quantum yields (ϕ_{sol}) were calculated relative to quinine sulfate ($\phi_{sol}=0.546$ in H_2SO_4 1 N) using standard procedures.[72] ϕ_{sol} was determined according to the following Equation (1), in which subscripts s and r refer to the sample and reference, respectively. The integrated area of the emission peak in arbitrary units is given as T, n is the refracting index of the solvent ($n_s=1.42662$ for cyclohexane and 1.469 for decalin; $n_r=1.3325$) and A is the absorbance. The emission spectra of DSF-IF, DSF-IF(iPr)$_2$, DSF-IF(oct)$_2$, SBF and F were recorded in solution in cyclohexane and IF in solution in decalin. IR spectra were recorded on a BIORAD IRFTS175C.

$$\phi_{sol} = \phi_{ref} \times 100 \times \frac{T_s A_r}{T_r A_s}\left(\frac{n_s}{n_r}\right)^2 \quad (1)$$

Thermal analysis: Thermogravimetric analyses (TGA) were performed with a Rigaku Thermoflex instrument under a nitrogen atmosphere. TGA measurements were carried out between 40 and 600 °C with a heating rate of 40 °C h^{-1} for IF and SBF and 5 °C min^{-1} for DSF-IFs. DSC measurements were carried out on a DSC 2010 TA instrument between 50 to 350 °C at a rate of 10 °C min^{-1} for DSF-IFs and at a rate of 40 °C min^{-1} for SBF and IF. Melting points were determined by using an electrothermal melting-point apparatus or by DSC.

Electrochemical studies: All electrochemical experiments were performed using a Pt disk electrode (diameter 1 mm), the counter electrode was a vitreous carbon rod and the reference electrode was a silver wire in a solution of $AgNO_3$ in CH_3CN (0.1 M). Ferrocene was added to the electrolyte solution at the end of a series of experiments. The ferrocene/ferrocenium (Fc/Fc^+) couple served as internal standard and all reported potentials were referenced to its reversible formal potential. All solvents were purchased from SDS with less than 100 ppm of water and stored under Argon. Activated Al_2O_3 was added in the electrolytic solution to remove excess moisture. The three-electrode cell was connected to a PAR Model 173 potentiostat monitored with a PAR Model 175 signal generator and a PAR Model 179 signal coulometer. The cyclic voltammetry traces (CVs) were recorded on an XY SEFRAM-type TGM 164. For a further comparison of the electrochemical and optical properties, all potentials are referred to the SCE electrode that was calibrated at −0.405 V versus Fc/Fc+ system in CH_2Cl_2. The peak potentials are given with an error of ±20 mV corresponding to 1 mm on the XY-Sefram recording table. Chemicals for electrochemistry: acetonitrile with less than 5‰ of water (ref. SDS 00610S21) and dichloromethane with less than 100 ppm of water (ref. SDS 02910E21) were used without purification. Tetrabutylammonium hexafluorophosphate from FLUKA was used without purification. Aluminum oxide was obtained from Woëlm, activated by heating at 300 °C under vacuum for 12 h and used at once under argon pressure.

X-ray structure determination: Crystal data and structure refinements for 2,2′DITP: $C_{18}H_{12}I_2$, M_r 482.08, crystal size 0.1×0.1×0.1 mm, colourless prism, orthorhombic, space group *Pbca*, $T=93(2)$ K, $a=11.2215(18)$, $b=8.0151(12)$, $c=16.796(3)$ Å, $V=1510.7(4)$ Å^3, $Z=4$, $\rho_{calcd}=2.120$ Mg m^{-3}, $\mu(Mo_{K\alpha})=4.150$ mm^{-1}, 8697 measured reflections, 1315 independent reflections (R_{int})=(0.0683), final $R1=0.0473$, $wR2=0.1007$ for 981 observed reflections [$I>2\sigma(I)$]. Crystal data and structure refinements for **11**: $C_{31}H_{22}O$, M_r 410.49, crystal size 0.1×0.1×0.01 mm, colourless platelet, orthorhombic, space group *Pbca*, $T=173(2)$ K, $a=14.901(2)$, $b=8.2947(12)$, $c=35.765(5)$ Å, $V=4420.6(11)$ Å^3, $Z=8$, $\rho_{calcd}=1.234$ Mg m^{-3}, μ ($Cu_{K\alpha}$)=0.562 mm^{-1}, 19222 measured reflections, 1707 independent reflections (R_{int})=(0.1798), final $R1=0.0780$, $wR2=0.1832$ for 1233 observed reflections [$I>2\sigma(I)$]. Crystal data and structure refinements for DSF-IF(iPr)$_2$: $C_{31}H_{22}O$, M_r 410.49, crystal size 0.18×0.18×0.1 mm, colourless prism, monoclinic, space group $P2_1$, $T=93(2)$ K, $a=9.7998(7)$, $b=14.8143(11)$, $c=15.1839(12)$ Å, $V=2111.6(3)$ Å^3, $Z=2$, $\rho_{calcd}=1.380$ Mg m^{-3}, $\mu(Mo_{K\alpha})=0.444$ mm^{-1}, 13187 measured reflections, 5575 independent reflections (R_{int})=(0.0153), final $R1=0.0236$, $wR2=0.0623$ for 5556 observed reflections [$I>2\sigma(I)$]. CCDC 653146, 653147 and 653148 contain the supplementary crystallographic data for this paper. These data can be obtained free of charge from The Cambridge Crystallographic Data Centre via www.ccdc.cam.ac.uk/data_request/cif.

EL fabrication and testing: OLEDs were fabricated using the following procedure.[103] Indium–tin oxide (ITO) substrates on glass from Merck underwent a solvent ultrasonic cleansing by using acetone and isopropanol followed by a 15 min UV-ozone treatment. A layer of poly(3,4-ethylene dioxythiophene) doped with poly(styrene sulfonate) (PEDOT/PSS from HC Starck) was then deposited onto ITO by spin-coating at 5000 rpm, from a 3 wt% water dispersion to form a 40 nm thick layer. PEDOT/PSS was subsequently annealed at 80 °C under vacuum for 30 min. This layer improves hole injection from the ITO to the HOMO level of the organic material and increases the performances and the lifetime of the device.[104] Then, the DSF-IF layer was thermally evaporated under vacuum (ca. 10^{-6} mbar) at a low deposition rate of 0.1 nm s^{-1}. The layer thickness was monitored in situ by a piezoelectric quartz balance during the evaporation. Calcium cathodes were finally evaporated through a shadow mask. The OLEDs were then stored and characterised under inert atmosphere in a nitrogen glove box ([O_2] and [H_2O]< 1 ppm). Contacts on ITO and Ca were taken using a probe (Karl Suss PM5). Current–voltage–luminance (I-V-L) curves were recorded using a Keithley 4200 SCS. Light emission was collected using a calibrated photodiode. Electroluminescence spectra were measured with a CCD spectrometer (Ocean Optics HR 2000).

Acknowledgements

The authors would like to thank the CINES (Centre Informatique National del'Enseignement Supérieur, Montpellier) for awarding of computing time, the C.R.M.P.O (Centre Régional de Mesure Physique del'Ouest) for high-resolution mass measurements and for CHN analysis. We also thank Dr. Muriel Hissler for helpful discussions and her help in fluorescence measurements and Stephanie Fryars for technical assistance.

[1] K. Müllen, U. Scherf, *Organic Light-Emitting Devices: Synthesis, Properties and Applications*, Wiley-VCH, Weinheim, **2006**.
[2] B. Geffroy, P. Le Roy, C. Prat, *Polym. Int.* **2006**, *55*, 572–582.
[3] D. Vak, B. Lim, S.-H. Lee, D.-Y. Kim, *Org. Lett.* **2005**, *7*, 4229–4232.
[4] E. Wang, C. Li, Y. Mo, Y. Zhang, G. Ma, W. Shi, J. Peng, W. Yang, Y. Cao, *J. Mater. Chem.* **2006**, *16*, 4133–4140.
[5] W. S. Shin, M.-K. Joo, S. C. Kim, S.-M. Park, S.-H. Jin, J.-M. Shim, J. K. Lee, J. W. Lee, Y.-S. Gal, S. A. Jenekhe, *J. Mater. Chem.* **2006**, *16*, 4123–4132.
[6] J. Jacob, S. Sax, T. Piok, E. J. W. List, A. C. Grimsdale, K. Müllen, *J. Am. Chem. Soc.* **2004**, *126*, 6987–6995.
[7] D. Vak, S. J. Shin, J.-H. Yum, S.-S. Kim, D.-Y. Kim, *J. Lumin.* **2005**, *115*, 109–116.
[8] F. Li, Z. Chen, W. Wei, Q. Gong, *Org. Electron.* **2005**, *6*, 237–241.
[9] K. L. Chan, M. J. McKiernan, C. R. Towns, A. B. Holmes, *J. Am. Chem. Soc.* **2005**, *127*, 7662–7663.
[10] H. P. Rathnayake, A. Cirpan, Z. Delen, P. M. Lahti, F. E. Karasz, *Adv. Funct. Mater.* **2007**, *17*, 115–122.
[11] H. Xiao, B. Leng, H. Tian, *Polymer* **2005**, *46*, 5707–5713.
[12] G. Jiang, B. Yao, Y. Geng, Y. Cheng, Z. Xie, L. Wang, X. Jin, F. Wang, *Macromolecules* **2006**, *39*, 1403–1409.
[13] K. Geramita, J. McBee, Y. Shen, N. Radu, D. T. Tilley, *Chem. Mater.* **2006**, *18*, 3261–3269.
[14] B. Huang, J. Li, J. Qin, Z. Jiang, G. Yu, Y. Liu, *Synth. Met.* **2005**, *153*, 261–264.
[15] B. Huang, J. Li, Z. Jiang, J. Qin, G. Yu, Y. Liu, *Macromolecules* **2005**, *38*, 6915–6922.
[16] H. P. Rathnayake, A. Cirpan, P. M. Lahti, F. E. Karasz, *Chem. Mater.* **2006**, *18*, 560–566.
[17] A. P. Kulkarni, Y. Zhu, S. A. Jenekhe, *Macromolecules* **2005**, *38*, 1553–1563.
[18] C.-L. Chiang, C.-F. Shu, C.-T. Chen, *Org. Lett.* **2005**, *7*, 3717–3720.
[19] Y. Jiang, J.-Y. Wang, Y.-X. Cui, Q.-F. Zhou, J. Pei, *Org. Lett.* **2006**, *8*, 4287–4290.
[20] Q. Zhou, A. Qin, Q. He, G. Lei, L. Wang, Y. Qiu, C. Ye, F. Teng, F. Bai, *J. Lumin.* **2007**, *122–123*, 674–677.
[21] J. Y. Shen, C. Y. Lee, T.-H. Huang, J. T. Lin, Y.-T. Tao, C.-H. Chen, C. Tsai, *J. Mater. Chem.* **2005**, *15*, 2455–2463.
[22] S. Chen, X. Xu, Y. Liu, W. Qiu, G. Yu, H. Wang, D. Zhu, *J. Phys. Chem. C* **2007**, *111*, 1029–1034.
[23] Z. H. Li, M. S. Wong, Y. Tao, J. Lu, *Chem. Eur. J.* **2005**, *11*, 3285–3293.
[24] K.-T. Wong, R.-T. Chen, F.-C. Fang, C.-C. Wu, Y.-T. Lin, *Org. Lett.* **2005**, *7*, 1979–1982.
[25] T. Hadizad, J. Zhang, Z. Y. Wang, T. C. Gorjanc, C. Py, *Org. Lett.* **2005**, *7*, 795–797.
[26] M. M. Elmahdy, G. Floudas, L. Oldridge, A. C. Grimsdale, K. Müllen, *ChemPhysChem* **2006**, *7*, 1431–1441.

[27] C. Tang, F. Liu, Y.-J. Xia, L. H. Xie, A. Wei, S.-B. Li, Q.-L. Fan, W. Huang, *J. Mater. Chem.* **2006**, *16*, 4074–4080.
[28] S. H. Lee, B.-B. Jang, Z. Kafafi, *J. Am. Chem. Soc.* **2005**, *127*, 9071–9078.
[29] M. J. Hancock, A. P. Gifford, Y. Zhu, Y. Lou, S. A. Jenekhe, *Chem. Mater.* **2006**, *18*, 4924–4932.
[30] C. Huang, C.-G. Zhen, S. P. Su, K. P. Loh, Z.-K. Chen, *Org. Lett.* **2005**, *7*, 391–394.
[31] Z. H. Li, M. S. Wong, H. Fukutani, Y. Tao, *Org. Lett.* **2006**, *8*, 4271–4274.
[32] W.-Y. Lai, R. Zhu, Q.-L. Fan, L.-T. Hou, Y. Cao, W. Huang, *Macromolecules* **2006**, *39*, 3707–3709.
[33] R. C. Chiechi, R. J. Tseng, F. Marchioni, Y. Yang, F. Wudl, *Adv. Mater.* **2006**, *18*, 325–328.
[34] S. Tao, S. Xu, X. Zhang, *Chem. Phys. Lett.* **2006**, *429*, 622–627.
[35] M. Kimura, S. Kuwano, Y. Sawaki, H. Fujikawa, K. Noda, Y. Taga, K. Takagi, *J. Mater. Chem.* **2005**, *15*, 2393–2398.
[36] F. I. Wu, C.-F. Shu, T.-T. Wang, E. W. G. Diau, C.-H. Chien, C.-H. Chuen, Y.-T. Tao, *Synth. Met.* **2005**, *1551*, 285–292.
[37] D. Berner, C. Klein, M. K. Nazeeruddin, F. De Angelis, M. Castellani, P. Bugnon, R. Scopelliti, L. Zuppiroli, M. Graetzel, *J. Mater. Chem.* **2006**, *16*, 4468–4474.
[38] S. Oyston, C. Wang, G. Hughes, A. S. Batsanov, I. F. Perepichka, M. R. Bryce, J. H. Ahn, C. Pearson, M. C. Petty, *J. Mater. Chem.* **2005**, *15*, 194–203.
[39] H.-Y. Wang, J.-c. Feng, G.-A. Wen, H.-J. Jiang, J.-H. Wan, R. Zhu, C.-M. Wang, W. Wei, W. Huang, *New J. Chem.* **2006**, *30*, 667–670.
[40] K.-T. Wong, T.-Y. Hwu, A. Balaiah, T.-C. Chao, F.-C. Fang, C.-T. Lee, Y.-C. Peng, *Org. Lett.* **2006**, *8*, 1415–1418.
[41] S. W. Culligan, A. C.-A. Chen, J. Wallace, K. P. Klubeck, C. W. Tang, S. H. Chen, *Adv. Funct. Mater.* **2006**, *16*, 1481–1487.
[42] Z. H. Li, M. S. Wong, *Org. Lett.* **2006**, *8*, 1499–1502.
[43] N. Leclerc, S. Sanaur, L. Galmiche, F. Mathevet, A.-J. Attias, J.-L. Fave, J. Roussel, P. Hapiot, N. Lemaître, B. Geffroy, *Chem. Mater.* **2005**, *17*, 502–513.
[44] V. Promarak, S. Saengsuwan, S. Jungsuttiwong, T. Sudyoadsuk, T. Keawin, *Tetrahedron Lett.* **2007**, *48*, 89–93.
[45] K. T. Kamtekar, C. Wang, S. Bettington, A. S. Batsanov, I. F. Perepichka, M. R. Bryce, J. H. Ahn, M. Rabinnal, M. C. Petty, *J. Mater. Chem.* **2006**, *16*, 3823–3835.
[46] K. Mouri, A. Wakamiya, H. Yamada, T. Kajiwara, S. Yamaguchi, *Org. Lett.* **2007**, *9*, 93–96.
[47] J. Jacob, J. Zhang, A. C. Grimsdale, K. Müllen, M. Gaal, E. J. W. List, *Macromolecules* **2003**, *36*, 8240–8245.
[48] S. Setayesh, D. Marsitzky, K. Müllen, *Macromolecules* **2000**, *33*, 2016–2020.
[49] P. Sonar, J. Zhang, A. C. Grimsdale, K. Müllen, M. Surin, R. Lazzaroni, P. Leclère, S. Tierney, M. Heeney, I. McCulloch, *Macromolecules* **2004**, *37*, 709–715.
[50] P. E. Keivanidis, J. Jacob, L. Oldridge, P. Sonar, B. Carbonnier, Balutschev, A. C. Grimsdale, K. Müllen, G. Wegner, *ChemPhysChem* **2005**, *6*, 1650–1660.
[51] T. P. I. Saragi, T. Spehr, A. Siebert, T. Fuhrmann-Lieker, J. Salbeck, *Chem. Rev.* **2007**, *107*, 1011–1065.
[52] D. Horhant, Ph.D. thesis, University of Rennes I (France), **2005**.
[53] D. Horhant, J.-J. Liang, M. Virboul, C. Poriel, G. Alcaraz, J. Rault-Berthelot, *Org. Lett.* **2006**, *8*, 257–260.
[54] R. G. Clarkson, M. Gomberg, *J. Am. Chem. Soc.* **1930**, *52*, 2881–2891.
[55] J. H. Weisburger, E. K. Weisburger, F. E. Ray, *J. Am. Chem. Soc.* **1950**, *72*, 4250–4253.
[56] J. H. Weisburger, E. K. Weisburger, F. E. Ray, *J. Am. Chem. Soc.* **1950**, *72*, 4253–4255.
[57] B. Winter-Werner, F. Diederich, V. Gramlich, *Helv. Chim. Acta* **1996**, *79*, 1338–1360.
[58] R. Wu, J. S. Schumm, D. L. Pearson, J. M. Tour, *J. Org. Chem.* **1996**, *61*, 6906–6921.
[59] Y. Fujioka, *Bull. Chem. Soc. Jpn.* **1984**, *57*, 3494–3506.
[60] M. L. Gross, D. H. Blank, W. M. Welch, *J. Org. Chem.* **1993**, *58*, 2104–2109.
[61] A. Suzuki, N. Miyaura, *Chem. Rev.* **1995**, *95*, 2457–2483.
[62] G. L. Stahl, R. Walter, C. W. Smith, *J. Org. Chem.* **1978**, *43*, 2285–2286.
[63] T. A. Kelly, D. W. McNeil, *Tetrahedron Lett.* **1994**, *35*, 9003–9006.
[64] G. Lecollinet, A. P. Dominey, T. Velasco, A. P. Davis, *Angew. Chem.* **2002**, *114*, 4267–4270; *Angew. Chem. Int. Ed.* **2002**, *41*, 4093–4096.
[65] C. Poriel, Y. Ferrand, S. Juillard, P. Le Maux, G. Simonneaux, *Tetrahedron* **2004**, *60*, 145–158.
[66] C. W. Lai, C. K. Lam, H. K. Lee, T. C. W. Mak, H. N. C. Wong, *Org. Lett.* **2003**, *5*, 823–826.
[67] B. M. Foxman, M. Rosenblum, V. Sokolov, N. Khrushchova, *Organometallics* **1993**, *12*, 4805–4809.
[68] W. C. Lothrop, *J. Am. Chem. Soc.* **1941**, *63*, 1187–1191.
[69] L. H. Xie, X.-Y. Hou, c. Tang, Y.-R. Hua, R.-J. Wang, R.-F. Chen, Q.-L. Fan, L.-H. Wang, W. Wei, B. Peng, W. Huang, *Org. Lett.* **2006**, *8*, 1363–1366.
[70] L. Mattiello, G. Fioravanti, *Synth. Commun.* **2001**, *31*, 2645–2648.
[71] L. Mattiello, L. Rampazzo, *J. Chem. Soc. Perkin Trans. 2* **1993**, 2243–2247.
[72] S. Merlet, M. Birau, Z. Y. Wang, *Org. Lett.* **2002**, *4*, 2157–2159.
[73] M. Czugler, J. J. Stezowski, E. Weber, *J. Chem. Soc. Chem. Commun.* **1983**, 154–155.
[74] J. Cuntze, L. Owens, V. Alcazar, P. Seiler, F. Diederich, *Helv. Chim. Acta* **1995**, *78*, 367–390.
[75] K.-T. Wong, T.-C. Chao, L. C. Chi, Y.-Y. Chu, A. Balaiah, S.-F. Chiu, Y.-H. Liu, Y. Wang, *Org. Lett.* **2006**, *8*, 5033–5036.
[76] K.-T. Wong, L. C. Chi, S.-C. Huang, Y.-L. Liao, Y.-H. Liu, Y. Wang, *Org. Lett.* **2006**, *8*, 5029–5032.
[77] H. Reisch, U. Wiesler, U. Scherf, N. Tuytuylkov, *Macromolecules* **1996**, *29*, 8204–8210.
[78] K.-T. Wong, Y.-L. Liao, Y.-T. Lin, H.-C. Su, C.-C. Wu, *Org. Lett.* **2005**, *7*, 5131–5134.
[79] Y.-H. Kim, D.-C. Shin, S.-H. Kim, C.-H. Ko, H.-S. Yu, Y.-S. Chae, S.-K. Kwon, *Adv. Mater.* **2001**, *13*, 1690–1693.
[80] Y. Wu, J. Li, Y. Fu, Z. Bo, *Org. Lett.* **2004**, *6*, 3485–3487.
[81] W.-J. Shen, R. Dodda, C.-C. Wu, F. I. Wu, T.-H. Liu, C.-H. Chen, C.-F. Shu, *Chem. Mater.* **2004**, *16*, 930–934.
[82] J. Rault-Berthelot, *Recent Res. Devel. Macromol. Res.* **1998**, *3*, 425–437.
[83] J. Rault-Berthelot, M. M. Granger, L. Mattiello, *Synth. Met.* **1998**, *97*, 211–215.
[84] W. Fu, J.K. Feng, G. B. Pan, *J. Mol. Structure (THEOCHEM).* **2001**, *545*, 157–165.
[85] R. Hoffmann, A. Imamura, G. D. Zeiss, *J. Am. Chem. Soc.* **1967**, *89*, 5215–5220.
[86] H. E. Simmons, T. Fukunaga, *J. Am. Chem. Soc.* **1967**, *89*, 5208–5214.
[87] B. H. Boo, Y. S. Choi, T.-S. Kim, S. K. Kang, Y. H. Kang, S. Y. Lee, *J. Mol. Struct.* **1996**, *377*, 129–136.
[88] A. Schweig, U. Weidner, D. Hellwinkel, W. Krapp, *Angew. Chem.* **1973**, *85*, 360–361; *Angew. Chem. Int. Ed. Engl.* **1973**, *12*, 310–311.
[89] A. Schweig, U. Weidner, R. K. Hill, D. A. Cullison, *J. Am. Chem. Soc.* **1973**, *95*, 5426–5427.
[90] P. Bischof, R. Gleiter, R. Haider, *J. Am. Chem. Soc.* **1978**, *100*, 1036–1042.
[91] N. L. Frank, R. Clérac, J.-P. Sutter, N. Daro, O. Kahn, C. Coulon, M. T. Green, S. Golhen, L. Ouahab, *J. Am. Chem. Soc.* **2000**, *122*, 2053–2061.
[92] Gaussian 03 (Revision C.02), M. J. Frisch, G. W. Trucks, H. B. Schlegel, G. E. Scuseria, M. A. Robb, J. R. Cheeseman, J. A. Montgomery Jr., T. Vreven, K. N. Kudin, J. C. Burant, J. M. Millam, S. S. Iyengar, J. Tomasi, V. Barone, B. Mennucci, M. Cossi, G. Scalmani, N. Rega, G. A. Petersson, H. Nakatsuji, M. Hada, M. Ehara, K. Toyota, R. Fukuda, J. Hasegawa, M. Ishida, T. Nakajima, Y. Honda, O. Kitao, H. Nakai, M. Klene, X. Li, J. E. Knox, H. P. Hratchian, J. B. Cross, C. Adamo, J. Jaramillo, R. Gomperts, R. E.

Stratmann, O. Yazyev, A. J. Austin, R. Cammi, C. Pomelli, J. W. Ochterski, P. Y. Ayala, K. Morokuma, G. A. Voth, P. Salvador, J. J. Dannenberg, V. G. Zakrzewski, S. Dapprich, A. D. Daniels, M. C. Strain, O. Farkas, D. K. Malick, A. D. Rabuck, K. Raghavachari, J. B. Foresman, J. V. Ortiz, Q. Cui, A. G. Baboul, S. Clifford, J. Cioslowski, B. B. Stefanov, G. Liu, A. Liashenko, P. Piskorz, I. Komaromi, R. L. Martin, D. J. Fox, T. Keith, M. A. Al-Laham, C. Y. Peng, A. Nanayakkara, M. Challacombe, P. M. W. Gill, B. Johnson, W. Chen, M. W. Wong, C. Gonzalez, J. A. Pople, Gaussian, Inc., Pittsburgh, PA, **2004**.

[93] P. Flükiger, H. P. Lüthi, S. Portmann, J. Weber, **2000**, MOLEKEL 4.0, Swiss Center for Scientific Computing, Manno (Switzerland).

[94] A. D. Becke, *J. Chem. Phys.* **1993**, *98*, 5648–5652.

[95] A. P. Kulkarni, C. J. Tonzola, A. Babel, S. A. Jenekhe, *Chem. Mater.* **2004**, *16*, 4559–4573.

[96] J. Tomasi, B. Mennucci, R. Cammi, *Chem. Rev.* **2005**, *105*, 2999–3093.

[97] C. Poriel, Y. Ferrand, P. Le Maux, J. Rault-Berthelot, G. Simonneaux, *Inorg. Chem.* **2004**, *43*, 5086–5095.

[98] C. Poriel, Y. Ferrand, P. Le Maux, C. Paul-Roth, G. Simonneaux, J. Rault-Berthelot, *J. Electroanal. Chem.* **2005**, *583*, 92–103.

[99] P. Hapiot, C. Lagrost, F. Le Floch, E. Raoult, J. Rault-Berthelot, *Chem. Mater.* **2005**, *17*, 2003–2012.

[100] L. Otero, L. Sereno, F. Fungo, Y.-L. Liao, C.-Y. Lin, K.-T. Wong, *Chem. Mater.* **2006**, *18*, 3495–3502.

[101] H. Lee, J. Oh, H. Y. Chu, J.-I. Lee, S. H. Kim, Y. S. Yang, G. H. Kim, L.-M. Do, T. Zyung, J. Lee, Y. Park, *Tetrahedron* **2003**, *59*, 2773–2779.

[102] Y. Imanishi, K. Fujita, Y. Miura, S. Kimura, *Supramol. Sci.* **1996**, *3*, 3–11.

[103] G. Wantz, L. Hirsch, N. Huby, L. Vignau, J. S. Silvain, A. S. Barrière, J. P. Parneix, *Thin Solid Films* **2005**, *485*, 247–251.

[104] A. van Dijken, A. Perro, E. A. Meulenkamp, K. Brunner, *Org. Electron.* **2003**, *4*, 131–141.

Received: July 5, 2007
Published online: November 19, 2007

